RSC Advances

Cite this: *RSC Advances*, 2012, **2**, 7384–7387

www.rsc.org/advances

COMMUNICATION

Hollow SnO_2 microspheres for high-efficiency bilayered dye sensitized solar cell

Jing Chen,†*[a] Chen Li,†[a] Feng Xu,†[b] Yidan Zhou,[a] Wei Lei,[a] Litao Sun[b] and Yan Zhang[c]

Received 11th May 2012, Accepted 27th June 2012
DOI: 10.1039/c2ra20909h

We synthesized hollow SnO_2 microspheres using a hydrothermal method and fabricated bilayered dye sensitized solar cells (DSSCs) with hollow SnO_2 microspheres as the top layer and TiO_2 as the bottom layer. Due to the reduced transfer resistance, faster diffusion constants, and enhanced light harvesting, the performance of the bilayered DSSC with SnO_2 top layer was better than that without SnO_2 top layer. A maximum power conversion efficiency (PCE) of 4.15% was obtained for this bilayered DSSC under illumination of one sun (AM 1.5 G, 100 mW cm^{-2}), which exhibited a 19% improvement compared to the QDSSC without a SnO_2 layer.

1. Introduction

Dye sensitized solar cells (DSSC) have received considerable research interest due to their low cost, simple fabrication process and relatively high conversion efficiencies[1–3].It is well accepted that the performance of DSSCs can be dominated by several factors, for example, the light harvesting ability of dyes, the electron transport rate at the semiconductor interface and the diffusion velocity of electrolyte. Compared to TiO_2, SnO_2 has a faster electron diffusion rate due to its higher electron-mobility (SnO_2, 125–250 $cm^2\ V^{-1}\ s^{-1}$; TiO_2, 0.1 ~ 1.0 $cm^2\ V^{-1}\ s^{-1}$)[4,5]. In addition, SnO_2 has other unique advantages suitable for a DSSC photoanode. For instance, the larger band gap for SnO_2 (3.6 eV) than TiO_2 (3.2 eV) can create fewer oxidative holes in the valence band to facilitate the long-term stability of DSSCs[6,7]. In addition, SnO_2 can be used as a reflecting layer, improving the photocurrent density and efficiency due to the Mie scattering effect[8].

However, few SnO_2 nanostructure based DSSCs have been reported and the efficiency is rather low. Qian *et al.* reported TiO_2 coated SnO_2 hollow microspheres as a bifunctional photoelectrode material in DSSCs for improving efficiency[6]. Koo *et al.* obtained over 10% efficiency for a DSSC with a nano-embossed hollow spherical TiO_2 particulate film as an overlayer on a nanocrystalline TiO_2 film[9]. Herein, we reported on the bilayered DSSC using hollow SnO_2 microspheres as the top layer and TiO_2 as the bottom layer. Taking advantage of the hollow SnO_2 structure, the photoanode within the SnO_2 hollow microspheres enhances the light harvesting due to multiple light reflections and scattering in the DSSC. Meanwhile, the bilayered photoanode can help improve the energy conversion efficiency by tuning the film structure from monolayer to multilayer[10]. The hollow SnO_2 microspheres were synthesized by a hydrothermal method. A power conversion efficiency (PCE) for the bilayered DSSC of 4.15% was obtained in this work.

2. Experimental

SnO_2 was synthesized through a hydrothermal method and the procedure was described elsewhere[11]. Briefly, 1.75 g Tin(IV) chloride, 1.71 g D–(+)-glucose, 10 ml deionized water, and 1 mmol or 5 mmol sulfuric acid were mixed together and reacted at 190 °C for 24 h. The precipitates were obtained and dried at 600 °C for 3 h. Two kinds of SnO_2 hollow microspheres with sizes of 200 nm and 600 nm were prepared. 0.5 g ethylcellulose was added to 5 ml ethanol and stirred for 30 min to form a clear gel. After that, 0.1 g SnO_2 powder and 0.4 g terpineol were added into the gel, and then stirred continually to form a homogenous white paste. A 10 μm thick TiO_2 film (Ti-Nanoxide T/SP, Solaronix) and a 2.0 μm thick SnO_2 film were deposited on FTO glass (SnO_2: F, Solaronix) sequentially by the doctor blading method. A bare 12 μm thick TiO_2 film was fabricated for comparison. Then, the electrodes were immersed into a 0.3 mM acetonitrile : *tert*-butyl alcohol (1 : 1) solution of *cis*-bis(isothiocyanato)(2,2′-bipyridyl-4,4′-dicarboxylato) (2,2′-bipyridyl-4,4′-dinonyl) ruthenium(II) (commercially called Z907 dye) for 3 h. The TiO_2/SnO_2 photoelectrodes were assembled with a 20 nm platinum-coated indium tin oxide (ITO) substrate as the counter electrode. The cell gap was maintained by a 60 μm thermal-plastic spacer. The iodide electrolyte consisting of 0.1 M LiI, 0.05 M I_2, 0.6 M 1-methyl-3-propylimidazolium iodide (MPII), and 0.5 M 4-*tert*-butyl-pyridine (TBP) in acetonitrile was injected into the cells by capillary effect. The area of the electrode was close to 0.16 cm^2. The photoanodes fabricated with TiO_2/SnO_2 (200 nm), TiO_2/SnO_2 (600 nm) and TiO_2 were named cell A, B and C, respectively.

X-ray diffraction (XRD) patterns were obtained on a D8 Advance X-ray diffractometer (Bruker AXS, USA) using Cu-Kα irradiation.

[a]*School of Electronic Science and Engineering, Southeast University, Nanjing, 210096, China. E-mail: chenjing@seu.edu.cn; Fax: +86-25-83792662; Tel: +86-25-83792650*
[b]*SEU-FEI Nano-Pico Center, Key Laboratory of MEMS of Ministry of Education, Southeast University, Nanjing, 210096, China. E-mail: fxu@seu.edu.cn*
[c]*Electrical Engineering Division, Engineering Department, University of Cambridge, 9 JJ Thomson Avenue CB3 0FA, Cambridge, UK. E-mail: yz236@cam.ac.uk*
† These authors contributed equally to this work.

Nitrogen adsorption–desorption isotherms were obtained on AS-6B apparatus (Micromeritics Instrument Corp.). All the samples were degassed at 150 °C prior to Brunauer–Emmett–Teller (BET) measurements. The thickness of the film was measured by TENCOR P-10 Surface Profiler. The absorption spectra were recorded using a SHIMADZU MPC-2200 UV-VIS Spectrometer. The current density-voltage (*J–V*) characteristics were measured with a Keithley 2440 Sourcemeter and the cell was subjected to the irradiation of a solar simulator (Abet-technologies, USA) operating at 100 mW cm^{-2} (AM 1.5 G). The incident photon to current conversion efficiency (IPCE) was measured with QE/IPCE Measurement Kit (Oriel, USA) in the wavelength range of 350 to 800 nm. Electrochemical impedance spectra (EIS) were measured under open circuit potential with oscillation potential amplitudes of 10 mV from 10^{-1} to 10^{6} Hz.

3. Results and discussion

3.1 Morphology and structure characterization of the photoanode

Fig. 1a and b show the scanning electron microscopy (SEM) images of the hollow SnO_2 microspheres with a size of ~600 nm. It is clearly seen that the SnO_2 has a hollow structure. Fig. 1c and d show the SEM images of the bare TiO_2 film and TiO_2/SnO_2 film. It can be seen that the 2 μm thick SnO_2 microsphere layer was uniformly dispersed on the 10 μm thick TiO_2 layer. Most SnO_2 microspheres has an open hole on the hollow structure after heat-treatment at 600 °C. Fig. 1e and f show the transmission electron microscopy (TEM) images of two kinds of SnO_2 microspheres. It is clear that both SnO_2 microspheres have a hollow structure with inner sphere

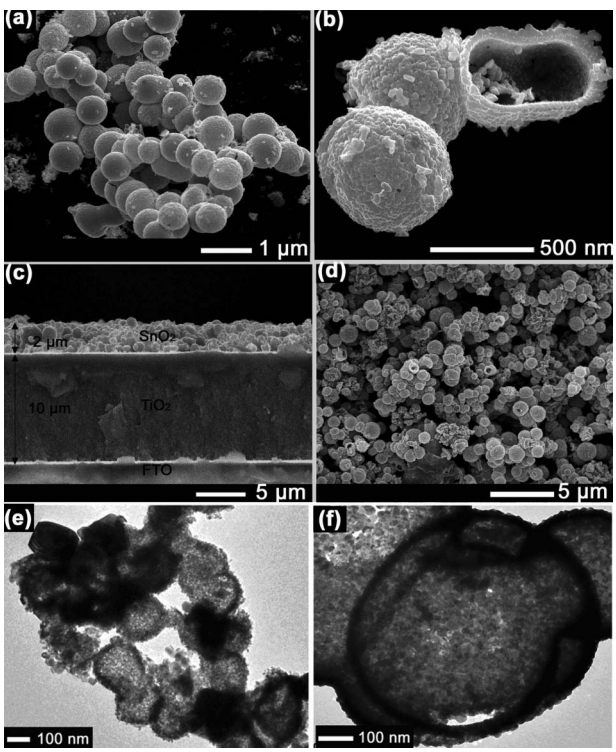

Fig. 1 (a) SEM image and (b) magnified image of 600 nm SnO_2 hollow microspheres (c) cross-section (d) top-view SEM image of TiO_2 coated with 600 nm SnO_2 film. TEM images of (e) 200 nm and (f) 600 nm SnO_2 hollow microspheres.

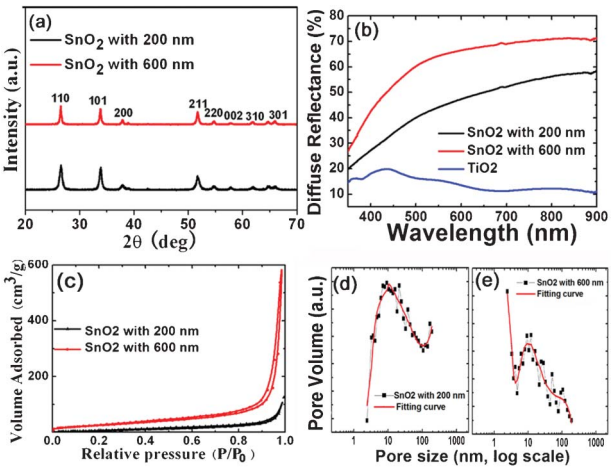

Fig. 2 (a) XRD pattern of 200 and 600 nm SnO_2 hollow microspheres. (b) Reflectance spectra of TiO_2/SnO_2 (200 nm), TiO_2/SnO_2 (600 nm), and TiO_2 (c) The N_2 adsorption and desorption isotherms of 200 and 600 nm SnO_2 powders. (d) and (e) Pore-size distribution of SnO_2 with 200 nm and 600 nm analyzed by N_2 adsorption.

diameters of 200 and 600 nm, respectively. And it has been reported that this hollow structure enhances light harvesting due its multiple light reflecting and scattering effects in the DSSC[6,9].

Fig. 2a shows the XRD spectra of 200 and 600 nm SnO_2 hollow microspheres. It can be seen that all the diffraction peaks of the SnO_2 hollow microspheres are in good agreement with a rutile structure of SnO_2 (JCPDS No.41–1445)[11]. Fig. 2b shows the reflectance measurement of TiO_2, TiO_2/SnO_2 (200 nm), and TiO_2/SnO_2 (600 nm). It can be seen that the reflecting light in hollow SnO_2 is higher than TiO_2. TiO_2 nanoparticles have very weak reflectance, and the light scattering effect is usually ignored due to their size being smaller than 30 nm[12]. Therefore, hollow SnO_2 can produce a greatly enhanced light harvest due to light multi-reflections and scattering. Fig. 2c shows the nitrogen adsorption and desorption isotherms of 200 nm and 600 nm SnO_2 powders. The BET surface areas for the 200 nm and 600 nm SnO_2 are 25.8 cm^3 g^{-1} and 93.5 cm^3 g^{-1}, respectively. The isotherm curves of 600 nm SnO_2 powder correspond to a hysteresis loop of type IV BDDT classification, indicating the presence of mesopores in the SnO_2 powder,[13–15] which can facilitate the transportation of the electrolyte and the adsorption of the dye in the DSSC[16]. Fig. 2d and e show the pore-size distribution for the SnO2 with 200 nm and 600 nm. The average pore size for SnO_2 is about 10 nm. The dye molecules adsorbed on cell A–C were desorbed by a 0.1 M NaOH solution (water : ethanol 1 : 1 vol%) for 24 h. The amounts of dye adsorption on cells A–C are calculated to be 6.6, 6.9 and 7.3 × 10^{-6} mol cm^{-2}, respectively.

3.2 Photovoltaic performances of DSSCs

Fig. 3a and b show *I–V* characteristics and the IPCE spectra of cells A–C at 100 mW cm^{-2} (AM 1.5 G), whose related photovoltaic parameters were listed in Table 1. Cell A has a PCE of 4.05% with short-circuit current density (J_{sc}) of 8.83 mA cm^{-2}, open-circuit voltage (V_{oc}) of 0.679 V, and fill factor (FF) of 67.6%. With 600 nm SnO_2 hollow microspheres (cell B) the DSSC leads to an improved PCE of 4.15% with J_{sc} = 9.36 mA cm^{-2}, V_{oc} = 0.662 V, and FF = 67.0%.

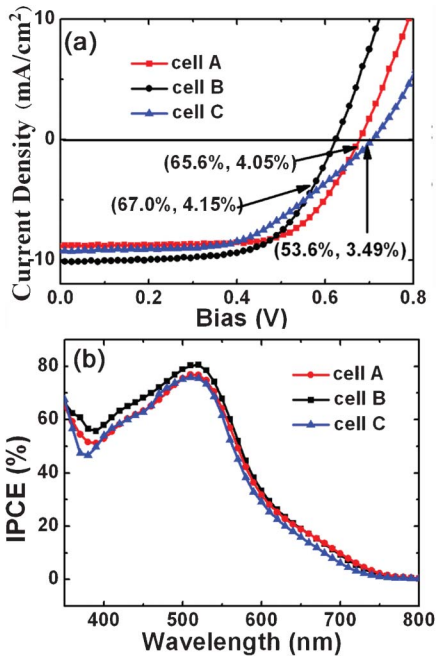

Fig. 3 (a) *I–V* characteristics (b) IPCE spectra of cell A–C measured under simulated solar illumination (AM 1.5 G) with an intensity of 100 mW cm^{-2} in iodide electrolyte. The corresponding values of FF and η are shown in the format of (FF, η) in (a).

Table 1 Detailed photovoltaic parameters of cell A–C

Cells	J_{sc} (mA cm^{-2})	V_{oc} (V)	FF	PCE
Cell A	8.83	0.679	67.6	4.05
Cell B	9.36	0.662	67.0	4.15
Cell C	9.23	0.706	53.6	3.49

Compared to cell C, the PCE of cell B has improved 19%, which is due to the increased J_{sc} and FF. The larger J_{sc} value for cell B is most likely because of enhanced light harvesting due to multiple light reflections within the TiO_2/SnO_2, rather than an increased surface area. Compared to cell C, the improvement in the FF values of cell A and B is due to the suppressed back electron transfer in the bilayered photoanodes. The V_{oc} for cells A and B were a little decreased. It is because the conduction-band edge of SnO_2 is 300 mV more positive than that of TiO_2, which leads to the decreased V_{oc} of cells with SnO_2 layer. Meanwhile, higher J_{sc} value for cell B than cell A should result from the larger dye absorption amount due to the enhanced surface areas, light scattering and reflection abilities. Therefore, cell B has the best performance among the three cells.

Fig. 3b presents the IPCE of cells A–C, which were measured in the wavelength range of 350 to 800 nm. The IPCE results are in good agreement with the PCE results shown in Fig. 3a. It can be seen that a maximum IPCE as high as 81% was obtained at 516 nm for cell B. The increment of IPCE for cell A and B is primarily due to the contribution of SnO_2 hollow microspheres forming a bilayered structure in the DSSC.

3.3 Diffusion constants and EIS measurements

Lastly, to reveal the kinetics of interfacial reactions of photoexcited electrons in DSSCs, we measured the EIS spectra of the as-prepared

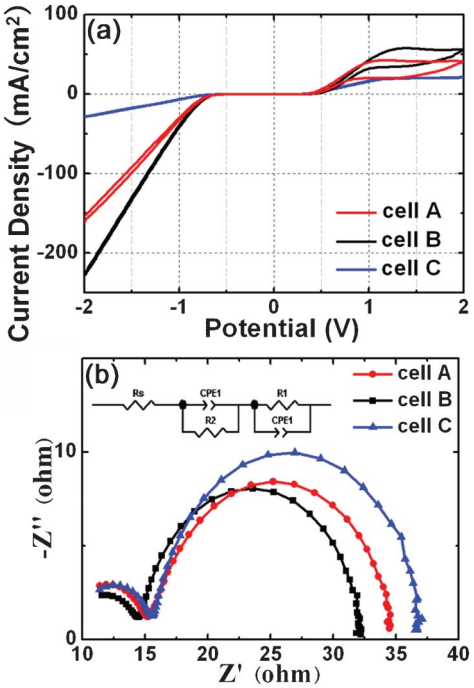

Fig. 4 (a) steady-state current–voltage curves of cells A–C. (b) Nyquist plots of cells A–C. The electric circuit is shown in the inset of Fig. 4b.

DSSCs. Fig. 4a shows the steady-state current–voltage curves of samples A–C. The diffusion-limited current density (j_{lim}) eqn (1) is shown as follows,[17]

$$j_{lim} = 2nFD_{I_3^-}c_{I_3^-}/l \quad (1)$$

Where F is Faraday's constant (96 484 C mol^{-1}), $c_{I_3^-}$ is the concentration per volume unit of I_3^-, $D_{I_3^-}$ is the diffusion constant of I_3^-, n is the number of electrons transported in the each reaction (in general, n = 2) and l is the distance between electrodes. The diffusion constants of I_3^- ($D_{I_3^-}$) for cells A–C are estimated as 2.0 × 10^{-6}, 2.9 × 10^{-6} and 1.6 × 10^{-6} cm^2 s^{-1}, respectively. Cell B has the highest diffusion constant among the three cells, which can be beneficial to the charge transfer in cell B.

Fig. 4b shows Nyquist plots of cells A–C at an applied bias of V_{oc} and a frequency range from 10^{-1} Hz to 10^6 Hz, with AC amplitude of 10 mV under the illumination of one sun (AM 1.5 G, 100 mW cm^{-2}). It can be seen that two semicircles were observed in the high-frequency region (>1k Hz) and middle-frequency region (10–100 Hz), respectively.

It was reported that the middle-frequency peak reflects the properties of the photoinjected electrons with the oxide semiconductor, which can be fitted to a transport resistance (R_w) and a constant phase element. The high-frequency peak can be fitted to a charge-transfer resistance (R_{ct}) and the chemical capacitance, which is due to charge transfer at the interfaces of the redox electrolyte/Pt counter electrode[18,19]. According to the electric circuit shown in the inset of Fig. 4b, the R_w and R_{ct} can be obtained by Z-view software. The R_w values are 19.6, 17.7 and 21.4 Ω and R_{ct} are 4.03, 2.07 and 4.33 Ω for cells A–C, respectively. Therefore, cell B performs the lowest value of R_w and R_{ct} among the three cells, indicating that more efficient charge transfer process at the interfaces of oxide/dye/electrolyte and electrolyte/Pt electrode[3,19]. The low resistance and high diffusion

constant in the DSSC can facilitate electron transfer and reduce electron recombination, leading to a higher FF value. As a result, the improved performance of DSSCs based on TiO_2 coated with hollow SnO_2 is ascribed to rapid charge transport with less diffusive hindrance by the presence of hollow SnO_2 microsphere layer.

4. Conclusion

Z907 dye sensitized solar cells based on SnO_2 hollow microspheres were studied in this work. A TiO_2/SnO_2/dye bilayered cell has a better performance than a TiO_2/dye cell, which is attributed to the multiple light reflection and scattering in the DSSCs by the presence of the SnO_2 hollow structure. EIS measurements demonstrated a lower resistance and faster diffusion constant for TiO_2/SnO_2/dye than TiO_2/dye, leading to the reduction of electron recombination and a lower FF value. As a result, a PCE of 4.15% was achieved for TiO_2/SnO_2/dye, which accounts for a 19% improvement compared to the TiO_2/dye cell.

References

1 E. Guillen, C. Fernandez-Lorenzo, R. Alcantara, J. Martin-Calleja and J. A. Anta, *Sol. Energy Mater. Sol. Cells*, 2009, **93**, 1846–1852.
2 S. Hore, C. Vetter, R. Kern, H. Smit and A. Hinsch, *Sol. Energy Mater. Sol. Cells*, 2006, **90**, 1176–1188.
3 K. Zhu, N. R. Neale, A. Miedaner and A. J. Frank, *Nano Lett.*, 2007, **7**, 69–74.
4 E. Hendry, M. Koeberg, B. O'Regan and M. Bonn, *Nano Lett.*, 2006, **6**, 755–759.
5 S. Gubbala, V. Chakrapani, V. Kumar and M. K. Sunkara, *Adv. Funct. Mater.*, 2008, **18**, 2411–2418.
6 J. F. Qian, P. Liu, Y. Xiao, Y. Jiang, Y. L. Cao, X. P. Ai and H. X. Yang, *Adv. Mater.*, 2009, **21**, 3663.
7 S. Chappel, S. G. Chen and A. Zaban, *Langmuir*, 2002, **18**, 3336–3342.
8 H. J. Koo, J. Park, B. Yoo, K. Yoo, K. Kim and N. G. Park, *Inorg. Chim. Acta*, 2008, **361**, 677–683.
9 H. J. Koo, Y. J. Kim, Y. H. Lee, W. I. Lee, K. Kim and N. G. Park, *Adv. Mater.*, 2008, **20**, 195–199.
10 Z. S. Wang, H. Kawauchi, T. Kashima and H. Arakawa, *Coord. Chem. Rev.*, 2004, **248**, 1381–1389.
11 H. X. Yang, J. F. Qian, Z. X. Chen, X. P. Ai and Y. L. Cao, *J. Phys. Chem. C*, 2007, **111**, 14067–14071.
12 J. Yu, J. Fan and K. Lv, *Nanoscale*, 2010, **2**, 2144–2149.
13 K. S. W. Sing, D. H. Everett, R. A. W. Haul, L. Moscou, R. A. Pierotti, J. Rouquerol and T. Siemieniewska, *Pure Appl. Chem.*, 1985, **57**, 603–619.
14 J. G. Yu, J. C. Yu, M. K. P. Leung, W. K. Ho, B. Cheng, X. J. Zhao and J. C. Zhao, *Journal of Catalysis*, 2003, **217**, 69–78.
15 J. G. Yu, G. H. Wang, B. Cheng and M. H. Zhou, *Appl. Catal., B*, 2007, **69**, 171–180.
16 S. Hore, P. Nitz, C. Vetter, C. Prahl, M. Niggemann and R. Kern, *Chem. Commun.*, 2005, 2011–2013.
17 A. Hauch and A. Georg, *Electrochim. Acta*, 2001, **46**, 3457–3466.
18 R. Kern, R. Sastrawan, J. Ferber, R. Stangl and J. Luther, *Electrochim. Acta*, 2002, **47**, 4213–4225.
19 Q. Wang, S. Ito, M. Gratzel, F. Fabregat-Santiago, I. Mora-Sero, J. Bisquert, T. Bessho and H. Imai, *J. Phys. Chem. B*, 2006, **110**, 25210–25221.